Implementation of the classical nucleation theory for precipitation

Michel Perez, Myriam Dumont, Daniel Acevedo-Reyes

Implementation of classical nucleation and growth theories for precipitation

M. Perez [a,*], M. Dumont [b], D. Acevedo-Reyes [c]

[a] *Université de Lyon, INSA Lyon, MATEIS: UMR CNRS 5510, F69621 Villeurbanne, France*
[b] *Université Paul Cézanne Aix-Marseille III, TECSEN: UMR CNRS 6122, F13397 Marseille, France*
[c] *CREAS, ASCOMETAL, BP 70045, 57301 Hagondange, France*

Three ways of implementing classical nucleation and growth theories for precipitation are presented and discussed: (i) the "mean radius approach" (particle size distribution is restricted to its mean radius and density); (ii) the "Euler-like multi-class approach" (the particle size distribution is discretized in several size classes and its time evolution is calculated evaluating the fluxes between neighboring classes); and (iii) the "Lagrange-like multi-class approach" (the particle size distribution is again discretized in several size classes, whose radius time evolution are calculated). In some simple cases, the three approaches lead to similar results, but when more complex heat treatments are involved, multi-class approaches are required. Although the Euler-like approach involves a more complex class number management, it is more adapted to the modeling of precipitate chemistry. Some examples of implementation are presented: Cu precipitation in ferrite, Al_3Sc precipitation in aluminum, VC and NbVC precipitation in austenite.

Keywords: Classical nucleation theory; Precipitation kinetics; Thermodynamics

1. Introduction

The precipitation of a second phase is widely used to enhance the properties of metallic alloys (strength, toughness, creep resistance, etc.). Age hardening [1] in aluminum alloys and grain size control in low alloyed steels [2] are two typical examples underlining the benefits of precipitation in metals.

Various approaches are being developed to predict the effect of thermomechanical treatments on the precipitation state. The relevant physical parameters describing these precipitates are: (i) their crystallography; (ii) their morphology; (iii) their chemical composition; (iv) their size distribution; (v) their volume fraction; and (vi) their number density.

* Corresponding author. Tel.: +33 4 72 43 80 63; fax: +33 4 72 43 85 39.
E-mail addresses: Michel.Perez@insa-lyon.fr (M. Perez), Myriam.Dumont@univ-cezanne.fr (M. Dumont), D.Acevedo@ascometal.lucchini.com (D. Acevedo-Reyes).

Among all the existing models, classical nucleation and growth theories (CNGTs) provide a compelling framework predicting the nucleation and growth rate of precipitates. When based on accurate thermodynamical functions, CNGTs are capable of describing the quantitative time evolution of the precipitation state, including parameters (iii)–(vi).

Despite the extensive amount of literature on CNGTs, the numerical implementation of nucleation and growth rate equations are seldom detailed. The aim of this paper is therefore to discuss and compare three classical ways of implementing CNGTs, namely:

(i) the "mean radius approach": in this approach, the particle size distribution (PSD) is restricted to its mean radius and density (number of precipitates per unit volume);
(ii) the "Euler-like multi-class approach": the PSD is discretized in several size classes and its time

evolution is calculated evaluating the fluxes between neighboring classes;

(iii) the "Lagrange-like multi-class approach":[1] the PSD is again discretized in several size classes, whose mean radius evolution is now calculated as a function of time.

First, CNGTs will be briefly reviewed with an emphasis on the two basic equations describing the nucleation and growth rates. Then, the three implementation techniques will be detailed and compared. Finally, the benefits and limits of each approach will be presented and illustrated through different examples in steels and aluminum alloys.

2. Classical nucleation and growth theories

2.1. Nucleation

Classical nucleation theory (CNT) is based on the changes in Gibbs energy ΔG associated with the formation of a precipitate in a supersaturated solid solution. In the case of spherical precipitates[2] of radius R, $\Delta G(R)$ is given by

$$\Delta G(R) = \frac{4}{3}\pi R^3 \Delta g + 4\pi R^2 \gamma \tag{1}$$

where Δg is the driving force for precipitation per unit volume and γ the specific interfacial energy (see Fig. 1).

CNGTs deal with (i) the rate at which stable nuclei ($R > R^*$) appear and (ii) the time evolution of the precipitate size distribution.

Nearly 80 years ago, Volmer and Weber [3] proposed the celebrated expression for the nucleation rate:

$$J_{\mathrm{VW}} \propto \exp\left[-\frac{\Delta G^*}{k_{\mathrm{B}}T}\right] \tag{2}$$

with ΔG^* being the energy required to form a critical nucleus of radius R^* (top of the nucleation barrier). Later, Becker and Döring [4] and Zeldovich [5] provided important insight into the kinetic nature of this pre-factor in Eq. (2), expressing the nucleation rate as

$$J_{\mathrm{BD}} = \beta^* N_0 Z \exp\left[-\frac{\Delta G^*}{k_{\mathrm{B}}T}\right] \tag{3}$$

where β^* is the condensation rate of solute atoms in a cluster of critical size R^* and N_0 is the number of nucleation site per unit volume and Z is the Zeldovich factor

$$Z = \frac{v_{\mathrm{at}}^{\mathrm{P}}}{2\pi R^*}\sqrt{\frac{\gamma}{k_{\mathrm{B}}T}} \tag{4}$$

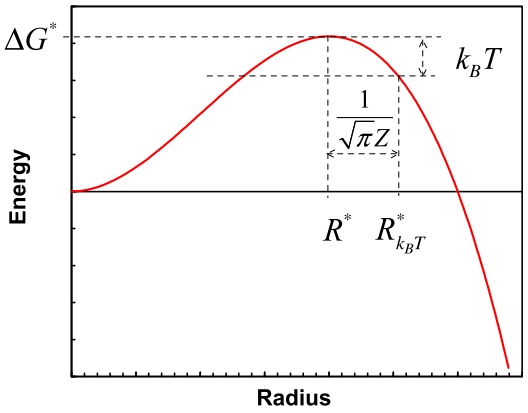

Fig. 1. Schematic representation of the Gibbs energy changes associated with precipitate formation as a function of their radius R in the classical nucleation theory. ΔG^* is the nucleation barrier, R^* is the critical radius for stable precipitates, $R^*_{k_{\mathrm{B}}T}$ is the radius at which stable precipitates nucleate and Z is the Zeldovich factor.

$v_{\mathrm{at}}^{\mathrm{P}}$ is the mean atomic volume within precipitates. Note that many expressions for the condensation rate β^* can be found in the literature, none of them being supported by a clear justification. Russell [6] proposed an expression[3] involving the diffusion coefficient of solute atoms D, the matrix mean solute atom fraction X and the lattice parameter a

$$\beta^* = \frac{4\pi R^{*2} D X}{a^4} \tag{5}$$

Kampmann and Wagner [7] introduced incubation time τ for nucleation, leading to the following expression for the nucleation rate:[4]

$$\left.\frac{\mathrm{d}N}{\mathrm{d}t}\right|_{\mathrm{nucl}} = N_0 Z \beta^* \exp\left(-\frac{\Delta G^*}{kT}\right)\exp\left(-\frac{\tau}{t}\right) \tag{6}$$

with $\tau = 4/(2\pi\beta^* Z^2)$. In their approach, the nucleus size is given by (see Fig. 1)

$$R^*_{k_{\mathrm{B}}T} = R^* + \frac{1}{\sqrt{\pi}Z} \tag{7}$$

2.2. Growth

In binary alloys, the diffusion controlled growth rate of spherical precipitates (molar composition X^{P}, radius R) embedded in a supersaturated solid solution (mean solute mole fraction in the matrix X, equilibrium solute mole fraction X^i at the precipitate/matrix interface) has been pro-

[1] The names "Euler" and "Lagrange" come from fluid mechanics, where lagrangian (one follows a particle) and Eulerian (fluxes are calculated at boundaries of a fixed box) approaches are used.

[2] The spherical shape of precipitates is an assumption that is used all along this paper.

[3] In multi-component precipitates, the addition of condensation characteristic times for each atomic species i gives

$$\beta^* = \frac{4\pi R^{*2}}{a^4}\left(\sum_i \frac{1}{D_i X_i}\right)^{-1}.$$

[4] The notion of "incubation time" can be, however, traced back much further than Kampmann's paper (starting with Turnbull [8]).

posed by Zener [9] under the assumption of small supersaturation ($X^0 - X^i \ll \alpha X^p - X^i$) and local equilibrium

$$\frac{dR}{dt} = \frac{D}{R}\frac{X - X^i}{\alpha X^p - X^i} \tag{8}$$

where $\alpha = v_{at}^M / v_{at}^P$ is the ratio of matrix to precipitates atomic volumes (mean volume per atom).

Interface curvature plays an important role on equilibrium mole fraction X^i, this is the so-called Gibbs–Thomson effect [10–14]. Hence, in a stoichiometric binary precipitate of composition A_xB_y, radius R and matrix/precipitate surface energy γ, precipitate/matrix interface equilibrium mole fractions X_A^i and X_B^i are modified [15]

$$X_A^i(R)^x X_B^i(R)^y = X_A^i(\infty)^x X_B^i(\infty)^y \exp\left(\frac{2\gamma(x+y)v_{at}^P}{Rk_BT}\right) \tag{9}$$

leading to the growth rate equation[5]

$$\left.\frac{dR}{dt}\right|_{growth} = \frac{D}{R}\frac{X - X^i(R)}{\alpha X^p - X^i(R)} \tag{10}$$

2.3. Coarsening

Eq. (9) naturally causes small precipitates to be less stable than large ones. At a constant volume fraction, small precipitates will then shrink (until complete dissolution) to the benefit of large ones, which will grow. This is the so-called coarsening mechanism that was investigated simultaneously by Lifchitz and Slyosov [17] and Wagner [18]. They proved that the PSD tends to a self-similar form (Lifshitz–Slyozov–Wagner (LSW) distribution) and managed to predict the mean radius evolution of a PSD from the Zener growth equation (Eq. (8)) and a linearized form of the Gibbs–Thomson equation (Eq. (9))

$$\left.\frac{d\overline{R}}{dt}\right|_{coars} = \frac{4}{27}\frac{X^i}{\alpha X^p - X^i}\frac{R_0 D}{\overline{R}^2} \tag{11}$$

where $R_0 = 2\gamma v_{at}^P/(k_BT)$. Note that, for the case of a stoichiometric binary precipitate of composition A_xB_y, the term R_0 of Eq. (11) should be replaced by $R_0(x+y)/y$.

2.4. Nucleation, growth and coarsening as concomitant processes

Langer and Schwartz described droplet formation and growth in near critical fluids (the LS model [19]). They treated nucleation, growth and coarsening as concomitant processes. They used steady-state nucleation theory and a linearized version of the Gibbs–Thomson equation (Eq. (9)), thus giving the time evolution of droplet density and mean radius ("Mean radius approach").

Later on, Kampmann and Wagner modified the Langer and Schwartz approach (the MLS model [7]) to treat precipitate formation and growth in supersaturated solid solution. As for the LS model, the MLS model does not account for the explicit form of the size distribution (the "mean radius approach").

More recently, Wagner and Kampmann have developed a numerical model (the KWN model [20]) that is capable of predicting the full evolution of the size distribution. The PSD is subdivided into intervals (size classes) and the continuous time evolution of the radius distribution function is split into a sequence of individual decomposition steps.

The KWN model has been extended and modified by many researchers. Myhr and Grong [21] presented a finite difference formulation of the KWN model by evaluating the fluxes between neighboring classes, the so-called "Euler-like multi-class approach". Nicolas and Deschamps studied non-isothermal treatments implementing the same approach [22].

The success of MLS or KWN models is largely due to their high versatility, covering a wide range of applications. The MLS model or "mean radius approach" has been used to model transition from metastable to stable phases [23] and heterogeneous nucleation on dislocations [24]. The "Lagrange-like multi-class approach" has been implemented to predict the chemistry of complex carbonitrides [25,16].

In the following section, the three ways of implementing CNGTs (namely "mean radius approach" and "Lagrange/Euler-like multi-class approach") will be detailed and discussed.

3. Multi-class vs. mean radius approaches

3.1. The mean radius approach

In the mean radius approach, we consider the time evolution of N precipitates of mean radius $\overline{R}$. Nucleation (Eq. (6)) and growth occur simultaneously. Note that the arrival of dN new nuclei of size $R^*_{k_BT}$ in the existing population of precipitates of radius $\overline{R}$ modifies the growth equation as follows:

$$\left.\frac{d\overline{R}}{dt}\right|_{growth} = \frac{D}{\overline{R}}\frac{X - X^i(\overline{R})}{\alpha X^p - X^i(\overline{R})} + \frac{1}{N}\frac{dN}{dt}\left(R^*_{k_BT} - \overline{R}\right) \tag{12}$$

In this approach, the coarsening stage, which is not implicitly taken into account by nucleation and growth equations (Eqs. (6) and (10)) requires specific expressions for precipitate number N and mean radius $\overline{R}$ evolution.

The LSW theory (Eq. (11)) describes the mean radius evolution in the asymptotic limit ($t \to \infty$). Within this limit, the solution mole fraction X is considered to be equal to the equilibrium solute mole fraction X^i. If the volume fraction of precipitates is small, the mass balance of solute atoms (total mole fraction X^0) is given by

$$X^0 = \alpha\frac{4}{3}\pi\overline{R}^3 N X^p + X\left(1 - \alpha\frac{4}{3}\pi\overline{R}^3 N\right) \tag{13}$$

[5] In multi-component precipitates, e.g. NbN, the growth process involves one growth equation per atomic species (see Ref. [16]).

Differentiation of Eq. (13) and use of LSW theory (Eq. (11)) gives the precipitate number density evolution during the pure coarsening stage:

$$\left.\frac{\mathrm{d}N}{\mathrm{d}t}\right|_{\mathrm{coars}} = \frac{4}{27}\frac{X^i}{\alpha X^{\mathrm{p}} - X^i} \times \frac{R_0 D}{\overline{R}^3}\left[\frac{R_0 X^i}{\overline{R}(X^{\mathrm{p}} - X^i)}\left(\frac{3}{4\pi\overline{R}^3} - N\right) - 3N\right] \quad (14)$$

In order to go continuously from the growth stage to the coarsening stage, Deschamps and Bréchet [26] introduced a coarsening fraction f_{coars} to weight the pure growth equation $\mathrm{d}\overline{R}/\mathrm{d}t|_{\mathrm{growth}}$ (Eq. (12)) and the pure coarsening equation $\mathrm{d}\overline{R}/\mathrm{d}t|_{\mathrm{coars}}$ (Eq. (11))

$$\frac{\mathrm{d}\overline{R}}{\mathrm{d}t} = f_{\mathrm{coars}}\left.\frac{\mathrm{d}\overline{R}}{\mathrm{d}t}\right|_{\mathrm{coars}} + (1 - f_{\mathrm{coars}})\left.\frac{\mathrm{d}\overline{R}}{\mathrm{d}t}\right|_{\mathrm{growth}} \quad (15)$$

They proposed an expression for the coarsening fraction

$$f_{\mathrm{coars}} = 1 - \mathrm{erf}\left[4\left(\frac{\overline{R}}{R^*} - 1\right)\right] \quad (16)$$

The last expression is well adapted to precipitation, but fails to describe precipitate dissolution ($\overline{R} < R^*$). In this paper, we choose a more general description (very close to the one proposed by Maugis [24])

$$f_{\mathrm{coars}} = 1 - 1000\left(\frac{\overline{R}}{R^*} - 1\right)^2 \quad 0.99R^* < \overline{R} < 1.01R^* \quad (17)$$

Similarly, the number of precipitates is given by

$$\begin{cases} \frac{\mathrm{d}N}{\mathrm{d}t} = f_{\mathrm{coars}}\left.\frac{\mathrm{d}N}{\mathrm{d}t}\right|_{\mathrm{coars}} & \text{if} \quad -\left.\frac{\mathrm{d}N}{\mathrm{d}t}\right|_{\mathrm{coars}} > \left.\frac{\mathrm{d}N}{\mathrm{d}t}\right|_{\mathrm{nucl}} \\ \frac{\mathrm{d}N}{\mathrm{d}t} = \left.\frac{\mathrm{d}N}{\mathrm{d}t}\right|_{\mathrm{nucl}} & \text{if} \quad -\left.\frac{\mathrm{d}N}{\mathrm{d}t}\right|_{\mathrm{coars}} < \left.\frac{\mathrm{d}N}{\mathrm{d}t}\right|_{\mathrm{nucl}} \end{cases} \quad (18)$$

The set of two equations for mean size $\overline{R}$ and number density N evolution (Eqs. (15) and (18)) can be integrated numerically using a Runge–Kutta scheme with adaptive time step. The solute fraction X, given by the mass balance (Eq. (13)) is re-evaluated at each time step.

3.2. Multi-class approaches: Euler vs. Lagrange

To describe the time evolution of the whole PSD, the continuous size distribution is discretized into a large number of size classes. A size class is defined by its radius R and the number of precipitates, the size of which ranges between $R - \Delta R/2$ and $R + \Delta R/2$.

From this definition, we can compute the total number of precipitates N per unit volume

$$N = \sum_i N_i \quad (19)$$

the mean radius of the distribution $\overline{R}$

$$\overline{R} = \frac{\sum_i R_i N_i}{\sum_i N_i} \quad (20)$$

and the precipitate volume fraction f_{T}

$$f_{\mathrm{T}} = \frac{4}{3}\pi\sum_i N_i R_i^3 \quad (21)$$

The mass balance is given by

$$X^0 = \alpha f_{\mathrm{T}} X^{\mathrm{p}} + X(1 - \alpha f_{\mathrm{T}}) \quad (22)$$

To model the evolution of the PSD, two strategies can be employed

- the exchange of particles between adjacent and predetermined size classes is calculated using a modified version of the growth equation (Eq. (10)) ("Euler-like multi-class approach");
- the radius evolution of each class (that contains a fixed number of precipitates) is calculated using directly the growth equation (Eq. (10)) ("Lagrange-like multi-class approach");

In the following, these two approaches will be presented in detail and compared with the "mean-radius approach".

3.3. The Euler-like approach

In the Euler-like approach, fluxes of particles at boundaries of fixed classes are evaluated. Such an approach is inspired by the KWN model.

3.3.1. Nucleation and growth

A nucleation stage is performed using the nucleation rate equation of the CNT (Eq. (6)). The number of new nuclei ΔN is given by

$$\Delta N = \frac{\mathrm{d}N}{\mathrm{d}t}\Delta t \quad (23)$$

where Δt is the time step. The size class in which to put these new nuclei is the one that contains the nucleation radius $R^*_{k_{\mathrm{B}}T}$.

The growth stage is computed using the control volume approach, as proposed by Myhr and Grong [21]. In this approach, the number density evolution of a size class i is evaluated from the number densities and growth rates of neighboring size classes (indexed $i-1$ and $i+1$), whose growth rates are $v_{i-1} = \mathrm{d}R/\mathrm{d}t|_{i-1}$ and $v_{i+1} = \mathrm{d}R/\mathrm{d}t|_{i+1}$. This case is illustrated in Fig. 2. The calculation of the particle number density within each class is highly dependent on the sign of the growth rate defined at the limits of the class i: $\mathrm{d}R/\mathrm{d}t|_{i-1}$ and $\mathrm{d}R/\mathrm{d}t|_i$. A mass balance gives the new population of class i

$$N_{i,t+\Delta t} = N_{i,t} + \frac{\Delta t}{\Delta R}v_{i-1,t}[\mathrm{SIGN}(v_{i-1,t})N_{i-1,t} + \mathrm{SIGN}(-v_{i-1,t})N_{i,t}] - \frac{\Delta t}{\Delta R}v_{i,t}[\mathrm{SIGN}(v_{i,t})N_{i,t} + \mathrm{SIGN}(-v_{i,t})N_{i+1,t}] \quad (24)$$

where the SIGN(x) function is 1 if $x > 0$ and 0 otherwise.

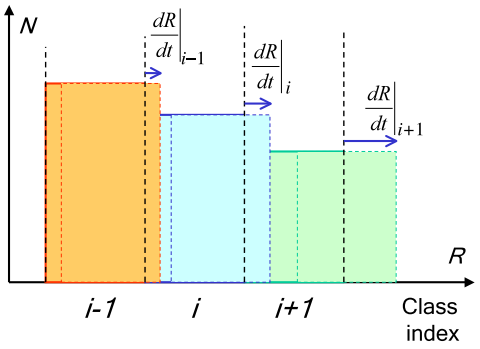

Fig. 2. Growth of precipitates in the "Euler-like approach". At each time step, fluxes between each neighboring classes are calculated.

3.3.2. Initial conditions

Computation is started with a system of size classes, the size and positions of which are predetermined. These classes can be either empty (no precipitates, $N_i = 0$) or represent a given PSD (e.g. coming from an experiment), for which we want to model the time evolution.

3.3.3. Time and boundary conditions

An auto-adapting time increment is calculated at each step of the process to avoid any size class moving more than one size element. Δt is calculated in such a manner that the class presenting the highest velocity $\mathrm{d}R/\mathrm{d}t_{\max}$ will move $\Delta R/2$

$$\Delta t = \frac{\Delta R}{2}\frac{1}{\mathrm{MAX}|\mathrm{d}R/\mathrm{d}t|_i|} \tag{25}$$

It should be noted that in practice $\mathrm{d}R/\mathrm{d}t|_{\max}$ is experienced by the smallest size class of the distribution, which is dissolving. For very small precipitates, infinite velocities can be calculated due to limitations of the assumptions involved in the growth rate equation. A cut-off value of the size distribution is then chosen to avoid the interfacial concentration becoming higher than the precipitate composition.

At the opposite end of the distribution, if the largest size class is in the growth regime, i.e. $\mathrm{d}R/\mathrm{d}t|_{i_{\max}}$ is positive, then at each time step a new size class will be created, even if $\mathrm{d}R/\mathrm{d}t|_{i_{\max}}$ is very small. At the next step this new size class, $i_{\max} + 1$, which may contain very few particles per unit volume (often less than 1 particle/m^3) will create another size class ($i_{\max} + 2$), and so on. Thus the number of classes would increase without limit, which would be impractical. To avoid this type of behavior inherent to Euler-like approach, a new size class can be created exclusively when the corresponding particle density is higher than a threshold (typically 1 particle/m^3). Otherwise the particles are left in their previous size class.

3.4. The Lagrange-like approach

The Lagrange-like approach is inspired by the "Multi-Préci" model developed by Maugis and Gouné [25]. In this approach, the time evolution of each size class radius is calculated, the size class population remaining constant. Hence, at each time step:

- a new class is created. Its radius is $R^*_{k_BT}$ and its population is

$$\Delta N = \left.\frac{\mathrm{d}N}{\mathrm{d}t}\right|_{\mathrm{nucl}} \Delta t \tag{26}$$

Nucleation rate is given by Eq. (6) and nucleation radius by Eq. (7). If ΔN is too low (typically lower than 10^{-10} times the total precipitate number density), no class is created.

- the new radius of all existing classes is calculated

$$R(t + \Delta t) = R(t) + \left.\frac{\mathrm{d}R}{\mathrm{d}t}\right|_{\mathrm{growth}} \Delta t \tag{27}$$

The growth rate is given by Eq. (10). Fig. 3 details how nucleation and growth stages are managed within the Lagrange-like approach.

3.4.1. Adaptive time step

In this approach, the time step drives the precision at which differential equations giving class numbers N_i and radii R_i are solved. Too short time step would lead to time-consuming calculations and unnecessarily large number of classes. Inversely, too long time step could lead to numerical instabilities (e.g. increasing amplitude oscillations around the solution) or even aberrations (e.g. negative concentrations).

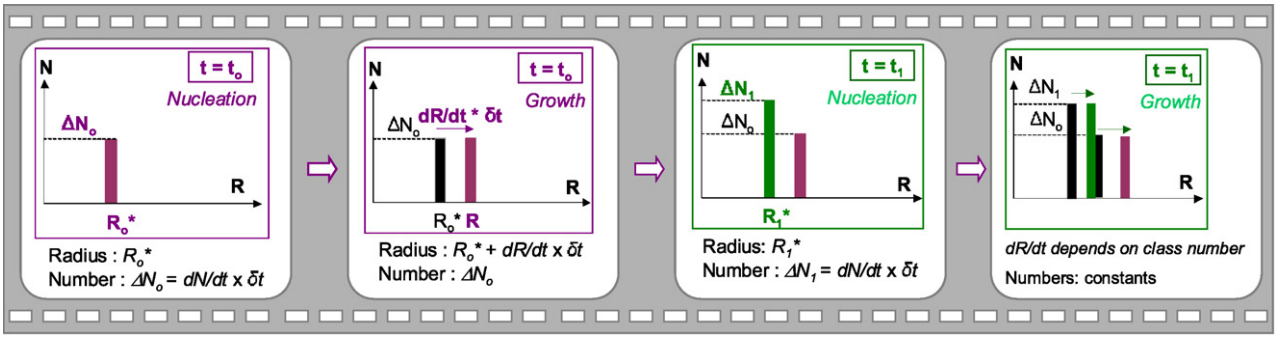

Fig. 3. Nucleation-growth sequence within a Lagrange-like approach. At each time step, a new class is created and all existing classes grow.

Thus, the time step needs to be optimized during the calculation. A logarithmic increment of the time step is first performed ($\Delta t \leftarrow 1.1\Delta t$). This new Δt is validated under two conditions, calculated at $t + \Delta t$:

- all solute concentrations should range between 0 and 1;
- the critical radius R^* (which is the most sensitive variable of the model) may not vary more than 1% between each time step.

If any of these conditions is not fulfilled, we return to the previous time step (this necessitates to keep in memory the state of the system at $t - \Delta t$) and make a new attempt with a smaller time step (typically $\Delta t \leftarrow \Delta t/2$). This last step could be repeated as many time as necessary.

Fig. 4 illustrates the adaptive time step scheme in the case of simultaneous precipitation of stable cementite and metastable ε carbides [23]. We observe that instabilities such as dissolution of precipitates lead to a strong decrease in the time step (see Fig. 4).

3.4.2. Class number management

In this approach, unlike in the Euler-like approach, the number of classes decreases during the coarsening stage:

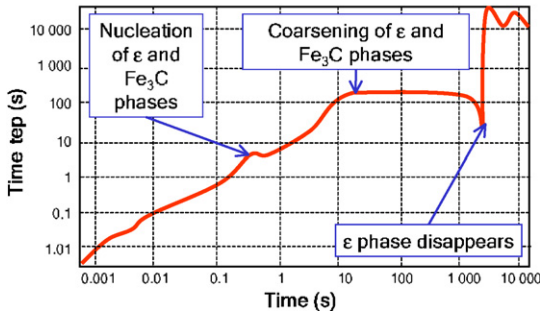

Fig. 4. Time-step evolution in the case of simultaneous precipitation of a metastable (ε carbide) and a stable (Fe_3C) phase in iron [23]. At approximately 1500 s, the time step is reduced to accurately model the complete dissolution of the metastable phase.

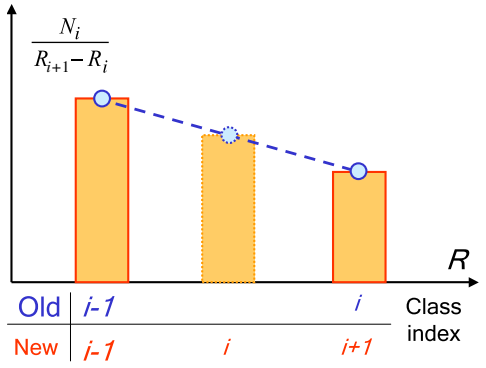

Fig. 5. Addition of a new class in the Lagrange-like approach. The new class should not modify the distribution density $N_i/(R_{i+1} - R_i)$.

classes smaller than the critical size ($R_i < R^*$) shrink, until they completely disappear. To keep an accurate description of the PSD, a minimum number of classes $N_{\min}$ should exist (typically $N_{\min} = 500$). Therefore, the maximum distance between two classes is fixed at

$$R_i - R_{i-1} > 2\frac{R_{\max} - R_{\min}}{N_{\min}} = \Delta R_{\max} \tag{28}$$

If the distance between two neighboring classes $i-1$ and i is higher than $\Delta R_{\max}$, a new class is artificially created. Insertion of a new class between classes $i-1$ and i would inevitably change either the mean radius $\overline{R}$ or the transformed fraction f_T. Indeed, rigorously keeping these two parameters would lead to a system of incompatible equations. Inserting a new class must lead to preservation of the distribution density $D_i = N_i/(R_{i+1} - R_i)$ rather than the distribution N_i.[6]

If a new class is added between classes $i-1$ and i, all classes with indices greater or equal to i are shifted up by one unit (see Fig. 5). The new class index is then i and the old class i becomes $i+1$. In the following, all indices are new indices.

It is then necessary to set new radii R'_{i-1}, R'_i, R'_{i+1} and populations N'_{i-1}, N'_i, N'_{i+1} of classes $i-1$, i and $i+1$ (six unknowns). We then suppose

- radii of old classes are kept unchanged

$$R'_{i-1} = R_{i-1} \quad \text{and} \quad R'_{i+1} = R_{i+1} \tag{29}$$

- the number densities of old classes are unchanged

$$D'_{i-1} = D_{i-1} \quad \text{and} \quad D'_{i+1} = D_{i+1} \tag{30}$$

- the new class is put right in the middle of the two old ones

$$R'_i = (R_{i-1} + R_{i+1})/2 \tag{31}$$

- continuity of the number density is provided

$$\frac{D'_i - D'_{i-1}}{R'_i - R'_{i-1}} = \frac{D'_{i+1} - D'_{i-1}}{R'_{i+1} - R'_{i-1}} \tag{32}$$

The above conditions lead to the new number of precipitates in each class

$$N'_{i-1} = 0.5N_{i-1} \quad N'_i = \frac{N_{i+1}}{4}\frac{R_{i+1} - R_{i-1}}{R_{i+2} - R_{i+1}} + \frac{N_{i-1}}{4} \quad N'_{i+1} = N'_{i+1} \tag{33}$$

The class insertion procedure cannot keep the precipitate volume fraction unchanged, which leads to a violation of the mass balance equation. To overcome this difficulty, after the transformation $[R_i, N_i] \rightarrow [R'_i, N'_i]$, a new transformation $[R'_i, N'_i] \rightarrow [R''_i, N''_i]$ has to be done in order to get a

[6] Note that if the time step had been half of its actual size during the nucleation stage, we would have had another class right inbetween classes $i-1$ and i (assuming a constant dR/dt), proving that only PSD density D_i has a physical meaning.

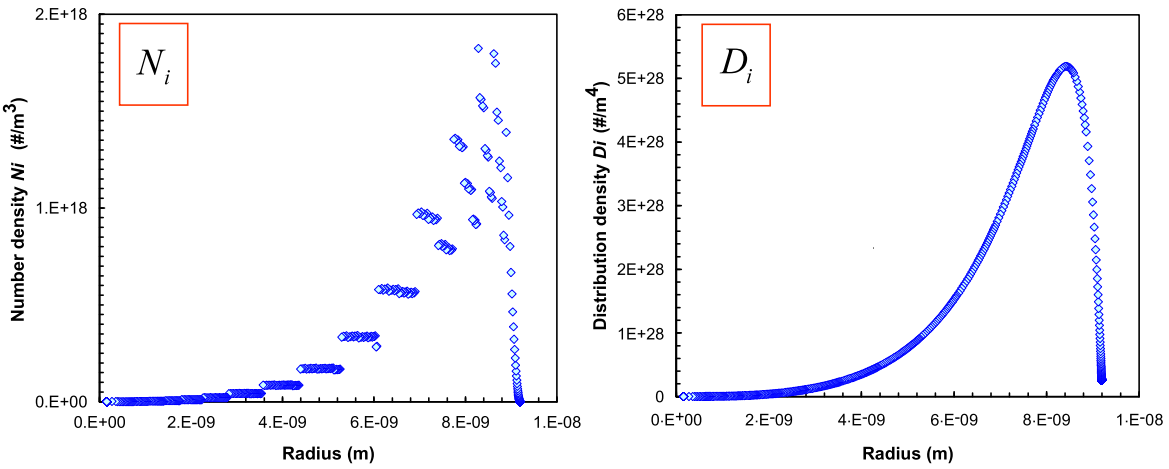

Fig. 6. Comparison between particle size distributions ($N_i = f(R)$) and particle size distribution density ($D_i = N_i/(R_{i+1} - R_i)$) after many insertions of new classes.

final precipitate volume fraction f_T'', which is rigorously equal to the initial precipitate volume fraction f_T.

$$f_T'' = \sum_i N_i'' R_i^{3''} = \sum_i N_i R_i^3 \tag{34}$$

This transformation consists in a rescaling of precipitate numbers N_i of all classes without changing their radii

$$R_i'' = R_i' \quad \text{and} \quad N_i'' = \xi N_i' \tag{35}$$

This naturally leads to

$$\xi = \frac{f_T}{f_T'} \tag{36}$$

Fig. 6 shows an example of particle size distribution $N_i(R_i)$ and distribution density $D_i(R_i)$. It can be observed that, unlike particle number density N_i, particle size distribution density $D_i = N_i/(R_{i+1} - R_i)$ remains smooth and unchanged after many class insertions.

3.5. Comparison between three approaches

To compare the three approaches presented above, we studied (i) simple nucleation-growth-coarsening kinetics involving homogeneous nucleation and (ii) a more complex situation where we compare two different PSDs with the same mean radius and precipitate transformed fraction.

3.5.1. A simple nucleation-growth-coarsening kinetics

In this example, the driving force for nucleation is given by an ideal solution model. We start with a supersaturated solid solution containing no precipitate. Parameters used to compare the three types of approaches (mean radius, Euler-like and Lagrange-like) are recalled in Table 1.

Fig. 7 compares evolutions of precipitate radii, precipitate number density, solute concentration and precipitate volume fraction for a nucleation-growth-coarsening sequence. The agreement between the three ways of implementing CNGTs is remarkable.

Table 1
Parameters used to compare the three types of approaches (mean radius, Euler-like and Lagrange-like) in the simple case of a nucleation-growth-coarsening sequence

X^p	X^0	X^i	D (m^2/s)	γ (J/m^2)	$v_{at}^{M,P}$ (m^3)	a (m)	T (°C)
1	0.06	0.01	5×10^{-20}	0.13	1.6×10^{-29}	4.04×10^{-10}	160

It is even surprising that the mean radius approach manages to describe so accurately the transition from nucleation-growth regimes to the coarsening regime. However, we will see in the next section that multi-class approaches are required in some more complex cases.

3.5.2. When the mean radius approach breaks down

A multi-class model definitely contains more information than a model dealing with mean quantities. However, the last section showed that the mean radius approach was as accurate in a simple case.

In some more complex situations, the mean radius approach breaks down. For example, in the case of a reversion treatment (i.e. a pre-existing PSD is submitted to high temperature treatment) a dissolution stage has been observed to occur without significant changes in the mean radius in Al–Zn–Mg alloys [22]. The mean radius approach is then expected to be unable to reproduce such a behavior since a decrease in the precipitate transformed fraction would involve a decrease in the mean radius.

Such kinds of complex treatments have been performed on a model Fe–0.2 wt.% V–0.5 wt.% C alloy, for which initial PSDs resulting from long-term treatment at 800 °C are submitted to thermal aging at 920 °C. In this section, we compare multi-class to mean radius approaches during a reversion treatment, starting from two different initial PSDs, which have the same mean radius and precipitate volume fraction. Therefore, the mean radius approach will not make any difference between these two PSDs.

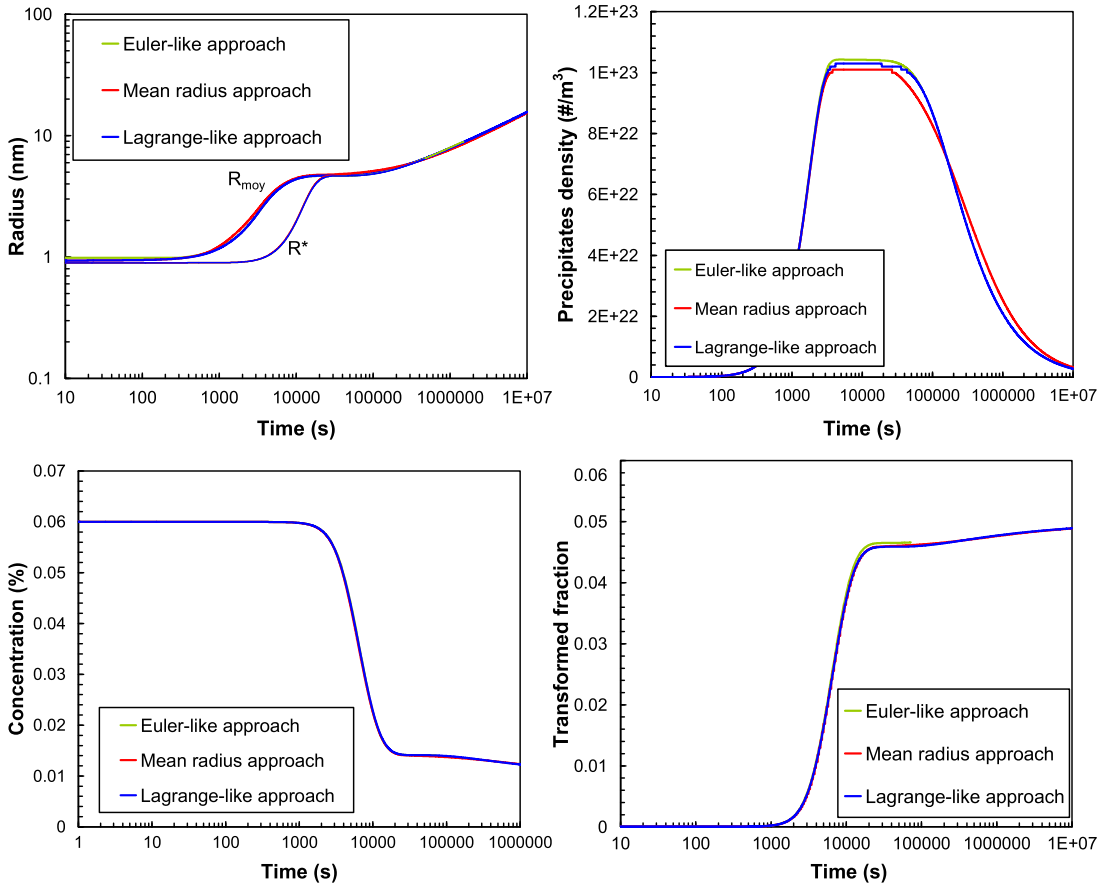

Fig. 7. Time evolution of radii, precipitate number density, solute concentration and precipitate volume fraction for multi-class and mean radius approaches. The agreement between the three ways of implementing CNGTs is remarkable.

Fig. 8a shows two initial distributions of VC precipitates in austenite resulting from a precipitation treatment of 10 days at 800 °C.[7] The first distribution is a classical LSW distribution resulting from a simulation involving nucleation-growth-coarsening stages (see parameters used for this model alloy in Table 2; more details can be found in Ref. [29]). The second distribution is an experimental one resulting from a fine scanning electron microscope characterization in the transmission mode (see Ref. [27]). Note that the experimental distribution has a log-normal shape in contradiction with the simulated one, which has an LSW shape.[8] In spite of their different shapes, these two distributions exhibit exactly the same mean radius and precipitate transformed fraction.

From these two distributions, an aging treatment at 920 °C is modeled with the three approaches: Lagrange-like, Euler-like and mean radius (see parameters in Table 2). The growth of precipitates is limited by vanadium diffusion; the equilibrium carbon fraction at the precipitate/matrix interface X_C^i is then equal to the carbon solute fraction X_C. The solubility product of vanadium carbides is given by: $K_{VC}(R) = K_{VC}\exp(R_0/R) = X_V^i X_C^i \exp(R_0/R)$ and the growth rate of the precipitates is

$$\frac{dR}{dt} = \frac{D_V}{R}\frac{X_V - X_V^i}{\alpha/2 - X_V^i} \tag{37}$$

Fig. 8b–d shows that the two initial PSDs give quite different results in terms of the mean radius (b), precipitate volume fraction (c) and precipitate number density (d) evolutions, especially for intermediate times. These differences can be perfectly explained by the different shapes of the PSDs and cannot be reproduced with the mean radius model. Indeed, the PSD that contains more small precipitates will experience more precipitate dissolution during the beginning of the coarsening stage, thus exhibiting a larger mean radius. From this example, it appears clearly that the mean radius approach is unable to predict a dissolution at constant mean radius as observed experimentally during reversion treatments.

It can be seen in Fig. 8b–d that both multi-class approaches lead to identical results, whereas the mean radius approach is in accordance with the two other approaches only for the LSW-type initial precipitate distribution.

[7] Although all observed vanadium carbide precipitates have been positively identified as monoclinic ordered V_6C_5 carbides [28], they will be considered, for the sake of simplicity, as stoichiometric carbides VC in this paper.

[8] This shape difference, reported many times in the literature, has, to our knowledge, never been explained.

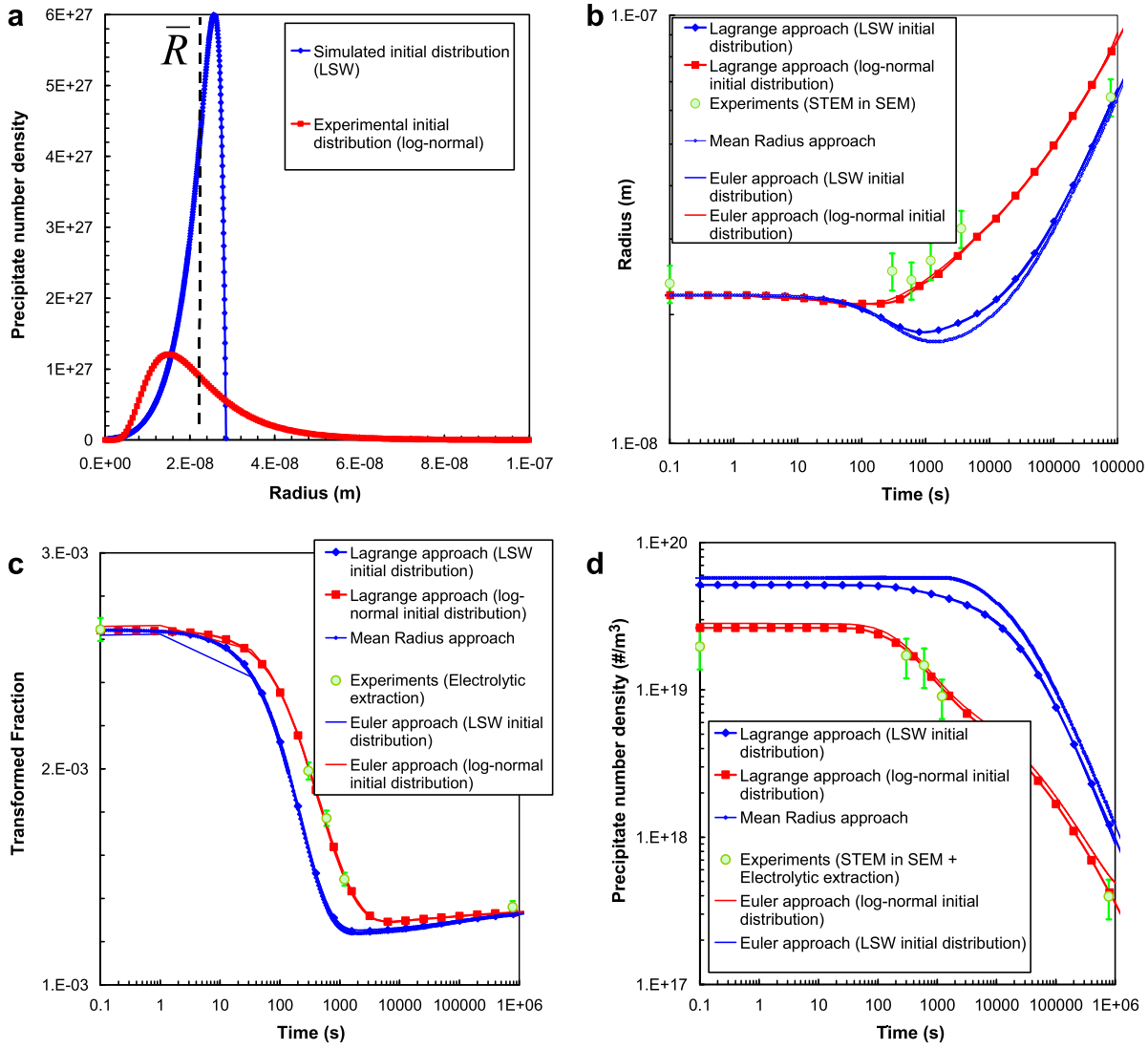

Fig. 8. (a) Precipitate size distribution resulting from a 10-day precipitation treatment at 800 °C: LSW distribution and experimental distribution [27] fitted by a log-normal function. These two distributions have the same mean radius AND precipitate volume fraction. Mean radius (b), transformed fraction (c) and number density (d) evolutions during an aging treatment at 920 °C for each the two distributions presented in (a): comparison between the three approaches. Both multi-class approaches are superimposed and fit remarkably well with experiments [27], whereas mean radius approach is unappropriate to model non-LSW precipitate size distribution.

Table 2
Parameters used to model the VC precipitate size distribution evolution of an FeVC model alloy

$\log_{10}K_{VC}$ [30]	D_V (m^2/s)[29]	γ (J/m^2)[29]	v_{at}^P (m^3)
$\frac{-9500}{T}+3.42$	$10^{-5}\exp(-\frac{240{,}000}{RT})$	0.4	9.9×10^{-30}

Indeed, equations that were used to build the LSW theory for coarsening (Eqs. (11) and (14)), on which the mean radius approach is based, suppose an LSW-type PSD. Therefore, the mean radius approach is unappropriate to model non-LSW precipitate size distribution evolution.

From Fig. 8b–d, finally, it can be noticed that experimental measurements (radii measured by scanning transmission electron microscopy (STEM) or scanning electron microscopy (SEM), and the transformed fraction with electrolytic extraction – for details see Ref. [31]) are in perfect agreement with both multi-class approaches providing that the initial PSD is an experimental log-normal distribution.

Such a reversion treatment has also been performed at 950 °C. The initial LSW distribution leads to a complete dissolution of all precipitates, whereas the biggest precipitates remain for the case of an initial log-normal distribution.

4. Applications

4.1. The mean radius approach: copper precipitation in iron

Precipitation of copper in iron has been extensively studied in the last 50 years because copper induces precipitation hardening after rapid cooling and tempering.

Despite the relative complexity of the precipitation sequence (body-centered cubic (bcc) → 9R → face-centered cubic (fcc)), the binary iron–copper system is quite often used as a model alloy to validate precipitation models, due to the spherical nature of precipitates and the fact that copper precipitates are reported to be pure copper even in the earlier stages of formation.

The LS model [32] and the N model [20] have been recently used on the binary Fe–Cu system to treat nucleation, growth and coarsening as concomitant processes. In this section, we will apply the mean radius approach to model the precipitation of copper in iron.

To take into account the loss of coherency on the precipitation kinetics, a size-dependent interfacial energy is introduced. As the bcc to fcc transition is usually observed for particles larger than $R_T = 3$ nm [20,33], the following form for γ has been chosen (see the inset of Fig. 9)

$$\gamma = \min\left[\gamma_{bcc} + \frac{R}{R_T}(\gamma_{fcc} - \gamma_{bcc}); \gamma_{fcc}\right] \tag{38}$$

All parameters used in this simulation are recalled in Table 3.

Fig. 9 shows the time evolution of precipitate mean radius and number density. The mean radius approach is compared with SANS [20,35] and SAXS experiments [33] performed on binary Fe–Cu alloys at 500 and 600 °C. The agreement is quite good in view of the simplicity of this approach: homogeneous nucleation, mean field approach, no impingement of precipitate diffusion fields (all precipitates lying within a solid solution, which solute fraction is updated at each time step).

4.2. The Euler-like approach: homogeneous nucleation of Al_3Sc in a dilute Al–Sc binary alloy

Pure homogeneous nucleation is rarely observed during aging of commercial alloys. Even an homogeneous distribution of precipitates as obtained in age-hardenable alloys has generally formed on homogeneously distributed defects such as vacancy-rich clusters or dislocations loops, so nucleation is heterogeneous in nature. Dilute Al–Sc binary alloys have proven to be a model system where pure homogeneous nucleation takes place [37]. Therefore the precipitation kinetics has been extensively studied in this system. Detailed experimental characterization [36,37] provided essential data for modeling which gave satisfactory results on the basis of classical nucleation and growth theory [37–39].

Table 3
Parameters used to model copper precipitation in iron

Parameter	Value	Reference
λX^p	1	
X^0	0.0125	
X^i	$\frac{5.77\times10^6}{T^2} - \frac{1.58\times10^4}{T} + 9.89$	[33]
D (m^2/s)	$6\times10^{-8}\exp\left(-\frac{166{,}400}{RT}\right)$	[34]
γ_{bcc} (J/m^2)	0.25	[20]
γ_{fcc} (J/m^2)	0.5	[20]
$v_{at}^{P,M}$ (m^3)	1.2×10^{-29}	

The object of the following example using the Euler-like approach applied to the nucleation of Al_3Sc precipitates in an Al–0.12 at.% Sc is to give an illustration on how a class model can help in understanding phenomenological processes. Novotny and Ardell [36] observed (see Fig. 10) that Al_3Sc precipitates were highly resistant to coarsening in this alloy. Even after long aging times (10^7 s) at 350 °C, precipitates do not undergo coarsening. Moreover, they observed that the particle size distribution (PSD) was in good agreement with the LSW prediction at early stages of aging, but the PSD became narrower than that predicted by the LSW theory for longer aging times. They conclude that this behavior was difficult to reconcile with the classical theory for nucleation, growth and coarsening.

The Euler-like approach was applied to this system using classical nucleation and growth theories. Parameters

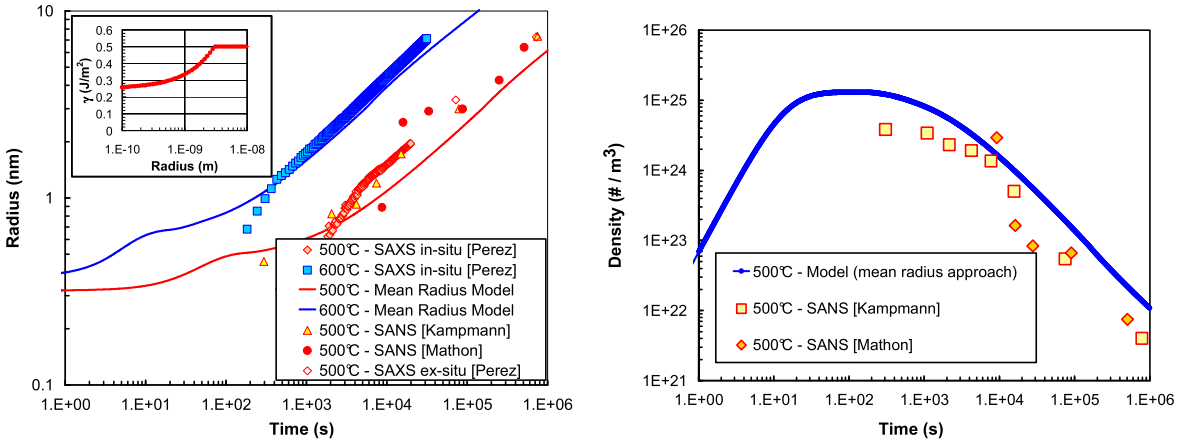

Fig. 9. Kinetic evolution of the precipitate radius (left) and number density (right) as predicted by the mean radius model. Solid points refer to experimental data from nuclear and magnetic SANS experiments on Fe–1.38 at.% Cu (from Wagner et al. [20] and Mathon et al. [35]), and SAXS experiments on Fe–1.25 at.% Cu (from Perez et al. [33]). Inset: to take into account the transition from the bcc coherent to the fcc incoherent phase, the precipitates interfacial energy varies from γ_{bcc} to γ_{fcc} depending on precipitate radius.

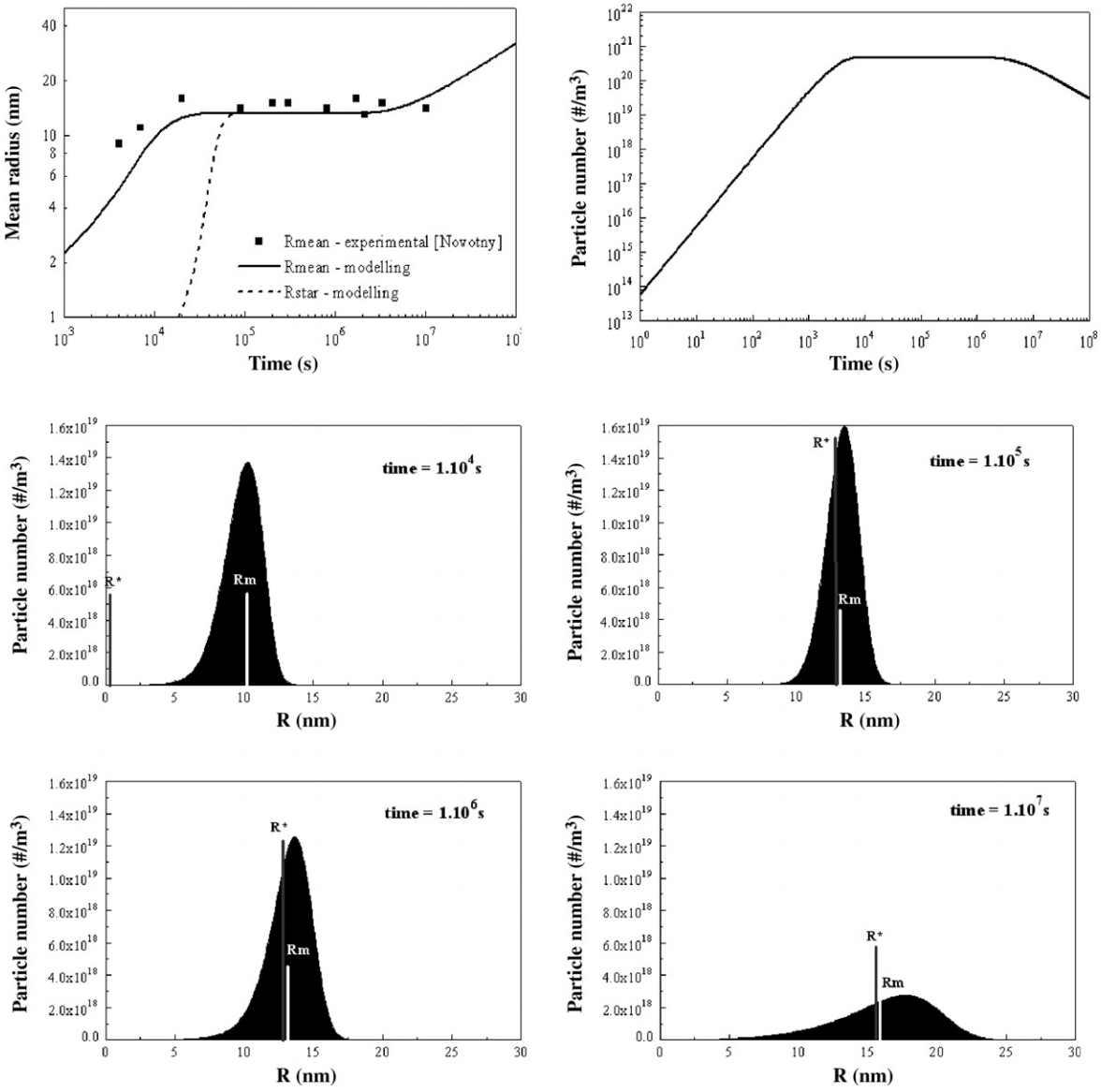

Fig. 10. Nucleation and growth of Al_3Sc precipitates in an Al–0.12 at.% Sc alloy during an isothermal treatment at 350 °C. Evolution of the average particle radius, as compared with Novotny and Ardell data [36], of the total number of precipitates and of the particle size distribution as predicted by the Euler-like multi-class model. Parameters used in the simulation: $\gamma = 0.127\ \mathrm{J\ m^{-2}}$, $D = 5.31 \times 10^{-4} \exp(-173,000/RT)\ \mathrm{m^2\ s^{-1}}$, $X_{Sc}(\infty) = 3.884 \times 10^{-5}$ at, $V_m^P = 4.166 \times 10^{-5}\ \mathrm{m^3\ mol^{-1}}$.

used in the model were extracted from the literature and are listed in the caption of Fig. 10. Only the interfacial energy was slightly adapted to fit at best the experimental data for two compositions (Al–0.12 and 0.18 at.% Sc) [36]. The retained value of $0.127\ \mathrm{J\ m^{-2}}$ is reliable with the values available in the literature [40,36,37,39] varying from 0.04 to $0.2\ \mathrm{J\ m^{-2}}$. The results obtained by modeling are in very good agreement with experimental data as shown on Fig. 10. In particular, modeling predicts a retardation of the coarsening stage in the dilute Al–0.12 at.% Sc alloy that starts for very long aging times: 10^7 s at 350 °C (last experimental data point). In this alloy, the nucleation stage characterized by the increase in the total particle number takes place over a large time scale, up to 10^4 s, because of the small supersaturation in this system. The transition from nucleation growth to a pure coarsening process is characterized by a constant mean radius stage. This plateau is generally predicted by modeling [26] but rarely observed experimentally since nucleation in commercial alloys is generally finished after a few minutes of aging. This stage proceeds until the decrease in the total number of precipitates starts, i.e. the set-up of the so-called coarsening stage.

From this example it appears that the criterion generally used to determine the beginning of the coarsening stage based on the R/R^* ratio is not satisfactory in this case. In fact, R^* closely approaches $\overline{R}$ early in the intermediate stage, i.e. 10^5 s, whereas the coarsening stage only begins after 10^6 s. The criterion $R^* \approx \overline{R}$ is a necessary condition that ensures the dissolution of the smallest particles that will supply solute atoms to the largest ones but appears

not to be sufficient. A second condition to satisfy is that the smallest particles have to be entirely dissolved to make the total number of particles decrease. In a global view of the PSD (see Fig. 10), it means that the PSD, relatively symmetrical at the transition from nucleation to growth stage ($\approx 10^5$ s), has to enlarge and generate small particle size classes before coarsening can begin. This takes quite a long time in the dilute Al–0.12 at.% Sc system because at the end of the nucleation-growth stage even the smallest precipitates are relatively large ($\approx$10 nm), and also involves a small dissolution rate. These two factors make them long to dissolve completely.

4.3. The Lagrange-like approach: (V, Nb)C dissolution in austenite

Microalloying elements such as Nb, V and Ti are commonly used in special steels because of the strong effect they can have on mechanical properties. A small addition of these elements leads to precipitation of carbides, nitrides and carbonitrides that can have a hardening effect or can control grain size growth. Enhancement of mechanical properties depends on the stability and evolution of the precipitation state during heat treatments.

In the specific case of vanadium and niobium carbides, the perfect miscibility of both carbides and the existence of a miscibility gap have been confirmed experimentally [41,42]. It has also been shown that the chemical composition of the mixed carbides formed depends on the size of the particles [43–45]. Hence, to model the evolution of the precipitation state, only a PSD-evolution model can be used.

A Lagrange-like approach has been used to model the evolution of the precipitation state during isothermal heat treatments in austenite of a FeCVNb model alloy. More details of the experimental characterization of the precipitation state will be published elsewhere. (V, Nb)C carbides are supposed to be stoichiometric for simplicity, and are modeled as a regular solution of VC and NbC:

$$\chi \mathrm{VC} + (1-\chi)\mathrm{NbC} \leftrightarrow \mathrm{V}_\chi \mathrm{Nb}_{1-\chi}\mathrm{C} \tag{39}$$

Growth and Gibbs–Thomson equations presented in Eq. (10) are written for (V, Nb)C precipitates as follows:

$$\begin{cases} \frac{\mathrm{d}R}{\mathrm{d}t} &= \frac{D_\mathrm{V}}{R}\frac{X_\mathrm{V}-X^i_\mathrm{V}}{\alpha\chi/2-X^i_\mathrm{V}} \\ \frac{\mathrm{d}R}{\mathrm{d}t} &= \frac{D_\mathrm{Nb}}{R}\frac{X_\mathrm{Nb}-X^i_\mathrm{Nb}}{\alpha(1-\chi)/2-X^i_\mathrm{Nb}} \\ \frac{\mathrm{d}R}{\mathrm{d}t} &= \frac{D_\mathrm{C}}{R}\frac{X_\mathrm{C}-X^i_\mathrm{C}}{\alpha/2-X^i_\mathrm{C}} \\ X^i_\mathrm{V}X^i_\mathrm{C} &= \chi K_\mathrm{VC}\exp\left(\frac{(1-\chi)^2\Omega^\mathrm{C}_\mathrm{VNb}}{k_\mathrm{B}T}\right)\exp\left(\frac{R_0}{R}\right) \\ X^i_\mathrm{Nb}X^i_\mathrm{C} &= (1-\chi)K_\mathrm{NbC}\exp\left(\frac{\chi^2\Omega^\mathrm{C}_\mathrm{VNb}}{k_\mathrm{B}T}\right)\exp\left(\frac{R_0}{R}\right) \end{cases} \tag{40}$$

The first three equations of system (40) drive the diffusion kinetics of V, Nb and C solute atoms. The last two equations define the solubility products of both VC and NbC carbides forming the complex $\mathrm{V}_\chi\mathrm{Nb}_{1-\chi}\mathrm{C}$ precipitate. The $\exp(R_0/R)$ stands for the Gibbs–Thomson effect and $\Omega^\mathrm{C}_\mathrm{VNb}$ is the interaction parameter of the regular solution model.

For the sake of simplicity, the χ dependence of α and R_0 have been neglected. System (40) is solved numerically using a Newton–Raphson scheme at each time step for all precipitate classes.

Parameters used for the simulation are presented in Tables 2 and 4. Initial PSD has been characterized combining TEM and SEM techniques [29].

Fig. 11 shows the evolution of $\mathrm{V}_\chi\mathrm{Nb}_{1-\chi}\mathrm{C}$ precipitate mean radius and chemical composition during isothermal holding at 950 and 1200 °C. Lagrange-like gives a good description of both mean radius and chemical composition.

Table 4
Parameters used to model the (Nb, V)C precipitate size distribution evolution of a FeNbVC model alloy

$\log_{10}K_\mathrm{NbC}$	D_Nb (m^2/s)	D_C (m^2/s)	γ (J/m^2)	$\Omega^\mathrm{C}_\mathrm{VNb}$ (J/mol)
$\frac{-7900}{T}+0.13$	$8.3\times10^{-5}\exp\left(-\frac{266{,}500}{RT}\right)$	$10^{-5}\exp\left(-\frac{137{,}500}{RT}\right)$	0.5	30,090

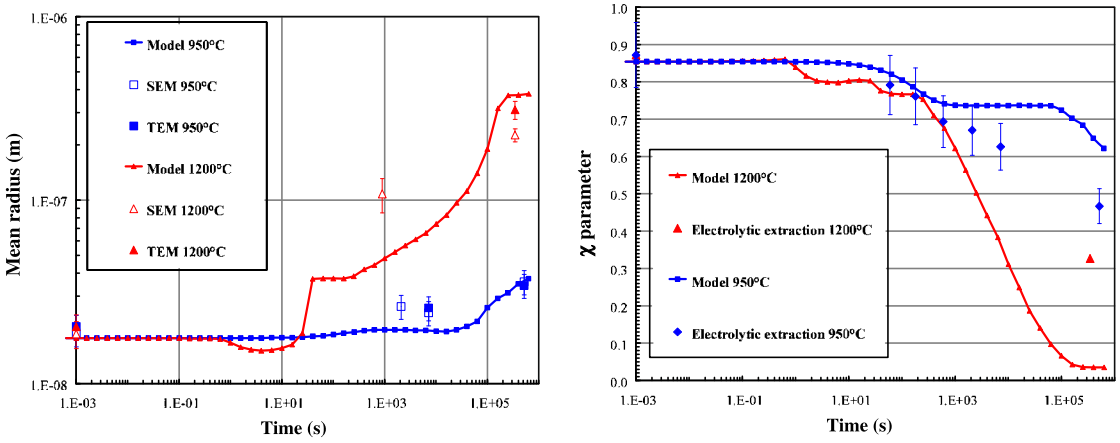

Fig. 11. Kinetic evolution of the precipitate radius (left) and chemical composition (right) as predicted by the Lagrange-like approach. Solid points refer to experimental data from SEM, TEM (precipitate radius) and electrolytic extraction (precipitate chemistry).

Just as for the case of Nb(C, N) precipitation in ferrite [16], the Lagrange-like approach is particularly well adapted to model the chemistry of precipitates. The reason is that all precipitates that appear at the same time shall have the same chemistry throughout all the precipitation treatment.

5. Conclusions

(1) On a simple nucleation-growth-coarsening sequence, mean radius and multi-class approaches are equivalent and give same results.
(2) In many relatively simple cases (precipitation sequence and thermal treatments), the mean radius approach is faster and as accurate as more complex multi-class approaches.
(3) The mean radius approach is unappropriate to model non-LSW precipitate size distribution evolution.
(4) A multi-class model is essential to take into account more complex treatments or shapes of the initial PSD: two different initial PSDs with the same (i) mean radius and (ii) precipitate volume fraction will actually lead to different mean radius evolution during a simulated aging treatment.
(5) To accurately describe the coarsening regime with a Lagrange-like approach, new classes should be added in the PSD. It is then necessary to keep the distribution density $D_i = N_i/(R_{i+1} - R_i)$ unchanged and to rescale all class populations to keep the precipitate volume fraction unchanged.
(6) The Euler-like approach has the advantage of not requiring a class number management as classes are fixed and delimited, but the optimal class size and position actually depends on the thermal treatment.
(7) The Lagrange-like approach offers better potentialities to model the chemistry of precipitates (e.g. precipitation of $V_xNb_{1-x}C$ or NbC_xN_y).

Table A.1
Table of symbols used in this paper

Symbol	Signification
α	Ratio of matrix to precipitates mean atomic volume $\alpha = v_{at}^{M}/v_{at}^{P}$
β^*	Condensation rate of solute atoms in a cluster of critical size R^*
Δg	Driving force for nucleation per unit volume
γ	Precipitate/matrix interfacial energy
ΔG	Gibbs energy change associated with the formation of a precipitate
ΔG^*	Nucleation barrier
Δt	Time step
τ	Incubation time $\tau = 4/(2\pi\beta^* Z^2)$
v_i	Growth rate of class i
a	Matrix lattice parameter
D	Diffusion coefficient of solute atoms
D_i	Precipitate size distribution density $D_i = N_i/(R_{i+1} - R_i)$
f_{coars}	Coarsening fraction
f_T	Precipitate transformed fraction
k_B	Boltzmann constant
N	Precipitate number density
N_i	Precipitate number density of class i
N_0	Number of nucleation site per unit volume
R	Precipitate radius
$\overline{R}$	Precipitate mean radius
R_0	Capillary radius $R_0 = 2\gamma v_{at}^{P}/(k_B T)$
R_i	Radius of class i
R^*	Critical radius for stable precipitates
$R^*_{k_B T}$	Nucleation radius
T	Temperature
$v_{at}^{M,P}$	Mean atomic volume within the matrix or precipitates
X	Solute mole fraction
X^0	Alloying element composition in mole fraction
X^i	Equilibrium solute mole fraction at the precipitate/matrix interface
X^p	Molar composition of precipitates
Z	Zeldovich factor

Acknowledgement

This work was partially supported by Ascometal CREAS. Thanks are due to P. Maugis, F. Perrard and A. Deschamps for fruitful discussions.

References

[1] Porter DA, Easterling KE. Phase transformation in metals and alloys. London: Chapman and Hall; 1992. 514p.
[2] Gladman T. The physical metallurgy of microalloyed steels. London: The Institute of Materials; 2002.
[3] Volmer M, Weber A. Keimbildung in übersättigen gebilden. Z Phys Chem 1926;119:277–301.
[4] Becker R, Döring W. Kinetische behandlung der keimbildung in übersättigten dämpfen. Annalen der Physik 1935;416:719–52.
[5] Zeldovich YB. On the theory of new phase formation: cavitation. Acta Physicochim USSR 1943;18:1–22.
[6] Russell KC. Phase transformations. American Society for Metals; 1968. p. 219–68 (Chapter Nucleation in solids).
[7] Kampmann R, Wagner R. Decomposition of alloys: the early stages. Pergamon Press; 1984. p. 91–103 (Chapter Kinetics of precipitation in metastable binary alloys – theory and application to Cu–1.9 at% Ti and Ni–14 at% Al).
[8] Turnbull D. Transient nucleation. Trans AIME 1948;175:774–83.
[9] Zener C. Theory of growth of spherical precipitates from solid solution. J App Phys 1949;20:950–3.
[10] Gibbs JW. Collected works. Green and Co.; 1928 (Chapter On the equilibrium of heterogeneous substances).
[11] Thomson J. Theoretical considerations on the effect of pressure in lowering the freezing point of water. Trans R Soc Edin 1849;16:575–80.
[12] Thomson J. On crystallization and liquefaction, as influenced by stresses tending to changes of form of crystals. Proc R Soc 1862;11:473–81.
[13] Thomson W. On the equilibrium of vapour at a curved surface of liquid. Phil Mag 1871;42:448–52.
[14] Thomson JJ. Application of dynamics to physics and chemistry. London: Macmillan; 1888.
[15] Perez M. Gibbs–Thomson effect in phase transformations. Scripta Mater 2005;52:709–12.
[16] Perez M, Courtois E, Acevedo D, Epicier T, Maugis P. Precipitation of niobium carbonitrides in ferrite: chemical composition measurements and thermodynamical modelling. Phil Mag Lett 2007;87:645–56.
[17] Lifchitz IM, Slyosov VV. The kinetics of precipitation from supersaturated solid solution. J Phys Chem Solids 1961;19(1/2):35–50.
[18] Wagner C. Theorie der alterung von niedershlSgen durch umlsen (ostwald-reifung). Z Electrochem 1961;65:581.

[19] Langer JS, Schwartz AJ. Kinetics of nuleation in near-critical fluids. Phys Rev A 1980;21:948–58.
[20] Wagner R, Kampmann R. Materials science and technology: a comprehensive treatment. John Wiley & Sons Inc.; 1991. p. 213–302 (Chapter Homogeneous second phase precipitation).
[21] Myhr OR, Grong O. Modelling of non-isothermal transformations in alloys containing a particle distribution. Acta Mater 2000;48: 1605–15.
[22] Nicolas M, Deschamps A. Characterisation and modelling of precipitate evolution in an Al–Zn–Mg alloy during non-isothermal heat treatments. Acta Mater 2003:6077–94.
[23] Perez M, Deschamps A. Microscopic modelling of simultaneous two-phase precipitation: application to carbide precipitation in low-carbon steels. Mater Sci Eng A 2003;A360:214–9.
[24] Perrard F, Deschamps A, Maugis P. Modelling the precipitation of NbC on dislocations in α-Fe. Acta Mater 2007;55:1255–66.
[25] Maugis P, Gouné M. Kinetics of vanadium carbonitride precipitation in steel: a computer model. Acta Mater 2005;53:3359–67.
[26] Deschamps A, Bréchet Y. Influence of predeformation on an ageing in an Al–Zn–Mg alloy – II Modeling of precipitation kinetics and yield stress. Acta Mater 1999;47(1):293–305.
[27] Acevedo-Reyes D, Perez M, Epicier T, Bogner A, Epicier T, Verdu C. Characterisation of precipitates size distribution: validation of low voltage STEM. J Micros 2008.
[28] Epicier T, Acevedo D, Perez M. Crystallographic structure of vanadium carbide precipitates in a model Fe–C–V steel. Phil Mag 2008;88:31–45.
[29] Acevedo D. Evolution de l'état de précipitation au cours de l'austénitisation d'aciers microalliés au vanadium et au niobium. PhD thesis, INSA Lyon; 2007.
[30] Narita K. Physical chemistry of the groups IVa (Ti, Zr), Va (V, Nb, Ta) and the rare earth elements in steel. Trans ISIJ 1975;15:145–52.
[31] Acevedo D, Perez M, Epicier T, Kozeschnik E, Perrard F, Sourmail T. Kinetics of precipitation and dissolution in model FeCV and FeCNbV alloy, and a microalloyed ultra high strength spring steel. In: New Dev. Metall. Appl. High Strength Steels. Bueno Aires: TMS; 2008.
[32] Zhang C, Enomoto M, Yamashita T, Sano N. Cu precipitation in a prestrained Fe1.5 wt pct Cu alloy during isothermal aging. Metall Trans A 2004;35A:1262–72.
[33] Perez M, Perrard F, Massardier V, Kleber X, Deschamps A, De Monestrol H, et al. Small angle X-ray scattering and tomographic atom probe. Phil Mag 2005;85(20):2197–210.
[34] Deschamps A, Nicolas M, Perrard F, Bley F. Non-isothermal precipitation kinetics in metallic alloys. In: Solid to solid phase transformations in inorganic materials. TMS; 2005.
[35] Mathon MH, Barbu A, Dunstetter F, Maury F, Lorenzelli N, de Novion CH. Experimental study and modelling of copper precipitation under electron irradiation in dilute FeCu binary alloys. J Nucl Mater 1997;245:224–37.
[36] Novotny GM, Ardell AJ. Precipitation of Al_3Sc in binary AlSc alloys. Mater Sci Eng A 2001;A318:144–54.
[37] Hyland RW. Homogeneous nucleation kinetics of Al_3Sc in a dilute Al–Sc alloy. Metall Trans A 1992;23A:1947–55.
[38] Robson JD. Modelling the overlap of nucleation, growth and coarsening during precipitation. Acta Mater 2004;52:4669–76.
[39] Clouet E, Nastar M, Sigli C. Nucleation of Al_3Zr and Al_3Sc in aluminum alloys: from kinetic Monte-Carlo simulations for classical theory. Phys Rev B 2004;69:064109.
[40] Jo H-H, Fujikawa S-I. Kinetics of precipitation in Al–Sc alloys and low temperature solid solubility of scandium in aluminium studied by electrical resistivity measurements. Mater Sci Eng A 1993;A171:151–61.
[41] Inoue K, Ishikawa N, Ohnuma I, Ohtani H, Ishida K. Calculation for phase equilibria between austenite and (Nb, Ti, V)(C, N) in microalloyed steels. ISIJ Int 2001;41:175–82.
[42] Kieffer R, Nowotny H, Neckel A, Ettmayer P, Usner L. Zur entmischung von kubischen mehrstoffcarbiden. Monatshefte fnr Chemie 1986;99:1020–7.
[43] Speer JG, Michael JR, Hansen SS. Carbonitride precipitation in niobium/vanadium microalloyed steels. Metall Trans A 1987;18A:211–22.
[44] Thompson SW, Krauss G. Precipitation and fine structure in medium-carbon vanadium and vanadium–niobium microalloyed steels. Metall Trans A 1989;20A:2279–88.
[45] Touryan LA, Thompson SW, Matlock DK, Krauss G. Microstructure and properties of medium-carbon steels microalloyed with vanadium and niobium. In: Finn M, editor. Proceedings of international symposium on microalloyed bar and forging steels. Montreal, Quebec: Canadian Institute of Mining and Metallurgy; 1990. p. 63–83.